


## Local chiral inversion of chiral nematic liquid crystals in cylinders

Shuting Li , Xuan Zhou,<sup>\*</sup> Jiliang Zhu, Kaiyang Du, Yike Du, and Han Gao  
*School of Science, Hebei University of Technology, Tianjin 300401, People Republic of China*



(Received 16 January 2023; accepted 3 March 2023; published 27 March 2023)

On the basis of Landau–de Gennes theory and the finite-difference iterative method, the autonomic modulation of chiral inversion in a cylindrical cavity with degenerate planar anchoring is investigated. Under the applied helical twisting power (inversely related to the pitch  $P$ ), a chiral inversion can be achieved due to the nonplanar geometry effect, and the inversion capacity rises with the increase of the helical twisting power. The combined effect of the saddle-splay  $K_{24}$  contribution (corresponding to the  $L_{24}$  term in Landau–de Gennes theory) and the helical twisting power are analyzed. It is found that the chiral inversion is more strongly modulated on the condition that the chirality of spontaneous twist is opposite to that of applied helical twisting power. Further, larger values of  $K_{24}$  will induce larger modulation of the twist degree and smaller modulation of the inverted region. The autonomic modulation of chiral inversion shows great potential for chiral nematic liquid crystal materials to be used in smart devices, such as light-controlled switches and nanoparticle transporters.

DOI: [10.1103/PhysRevE.107.034705](https://doi.org/10.1103/PhysRevE.107.034705)

### I. INTRODUCTION

Chiral nematic liquid crystals (CLCs) are fluid flexible media that are often used as electro-optical materials in a wide range of display applications [1,2]. In particular, CLCs confined in cylindrical cavities can be used as mood rings, thermometer strips [3,4] and eWriters [5], etc. In addition, as responsive materials, the reflection bands of CLCs can be adjusted according to the closed cylindrical surface and the external perturbations [6–13].

Different from nematic liquid crystals, CLCs exhibit the self-organized helical structure. From the macroscopic level, the liquid crystal molecules are arranged in layers, with the average orientation of each layer rotated by a small angle, and the distance between the two layers is the helical pitch  $P$  after achieving a total rotation of  $360^\circ$  [14]. At the microscopic level, this is the result of a composition of chiral molecules [15,16]. When the light propagates along the helical axis, the incident light will be selectively reflected, and the corresponding reflection peak wavelength is  $\lambda_0$ ,  $\lambda_0 = nP$ , where  $n$  is the average refractive index of liquid crystal. Obviously, the key to control the reflection wavelength is to change the helical pitch  $P$  sensitive to the environment. Typically, an early dual-probe fiber sensor was made by Yang *et al.* [17] from cholesteryl derivatives encapsulated in a cylindrical coupler device to monitor volatile organic compound gas using the principle that short-range interactions between volatile gas molecules and CLCs result in the variation of  $P$  [18–21]. Later, devices such as thermometers, lasers, and biosensors emerged [22–24]. These devices ultimately manipulate reflected light by changing the helical pitch  $P$ , with controllable environmental factors including external stimuli such as elec-

tric field and temperature and internal parameters such as the saddle-splay elasticity constant  $K_{24}$  [25–27].

Recent experiments by Jonghee Eun *et al.* [28] have achieved the chirality modulation of helical structures in capillaries, leading to a new stage in the study of CLCs. The unusual elastic properties of nematic lyotropic chromonic liquid crystals (LCLCs), i.e., the large saddle-splay elastic constants  $K_{24}$  compared to the twisted elastic constants  $K_{22}$ , responsible for chiral symmetry breaking to reduce the total elastic free energy [29–33] allow LCLCs to spontaneously form two chiral double twisted structures, and the addition of specific concentrations of chiral dopants with the opposite chirality results in a chiral inversion of the twisted structure. It means that excess chiral amino acids can be easily detected by optical observation, which lays the foundation for the application of CLCs in chiral molecular separators.

Up to now, the single function of twist degree modulation and chirality modulation for CLCs has been achieved independently. It remains difficult to realize the autonomous modulation of chiral inversion, including inverted region and twist degree both in one device, and it is difficult to fully characterize the fine structures of chiral structure. Inspired by this, we have examined in detail the modulation process for CLCs in cylinders with a degenerate planar anchoring, based on Landau–de Gennes theory.

This paper is organized in the following manner. In Sec. II we describe how we model the liquid crystal and briefly describe our numerical methods. To achieve our aim we have divided our study into three stages, which are presented in Sec. III. First, we consider the chiral structure due to the single effect of nonplanar geometry. Second, based on two kinds of spontaneous twist structure, the modulation ability of the helical twisting force is analyzed, including the chiral inversion region and the distortion degree. Finally, the influence of  $K_{24}$  on the modulation ability is explored. We summarize our results in Sec. IV.

<sup>\*</sup>Corresponding author: [zhouxuan198536@163.com](mailto:zhouxuan198536@163.com)

## II. THEORETICAL BASIS

### A. Free energy expression

The numerical procedure to obtain the chiral structure is almost the same as that employed in our previous studies [26,27]. We employ the second-rank symmetric and traceless tensor  $Q$  in Landau-de Gennes theory [34–36]. The Landau-de Gennes free energy density of liquid crystal is given by  $f = f_{\text{bulk}} + f_{\text{elastic}}$ , where  $f_{\text{bulk}}$  is the bulk energy, and its expression is the same as that in Refs. [26,27],

$$f_{\text{bulk}} = \frac{1}{2}A\text{tr}Q^2 - \frac{1}{3}B\text{tr}Q^3 + \text{tr}\frac{1}{4}C(\text{tr}Q^2)^2. \quad (1)$$

The free energy  $f_{\text{elastic}}$ , which penalizes gradients in the tensor order parameter field, is given in the form [36,37]

$$f_{\text{elastic}} = \frac{1}{2}\{L_1|\nabla Q|^2 + L_2|\nabla \cdot Q|^2 + L_{24}\nabla \cdot [(\nabla Q)Q - Q\nabla \cdot Q] + 2L_5q_0Q \cdot (\nabla \times Q)\}, \quad (2)$$

in which  $L_1$ ,  $L_2$ , and  $L_{24}$  are elastic constants, and  $L_5$  is a chiral term, estimated from measurement of the elastic constants from the Frank free energy density [37],

$$f_{\text{frank}} = \frac{1}{2}\{K_{11}(\nabla \cdot n)^2 + K_{22}(n \cdot \nabla \times n + q_0)^2 + K_{33}(n \times \nabla \times n)^2 - (K_{24} + K_{22})\nabla \cdot [n(\nabla \cdot n) + n \times \nabla \times n]\}, \quad (3)$$

in Eqs. (2) and (3),  $q_0 = \frac{2\pi}{P}$ .

Under the assumption of uniaxial  $Q$  and uniform  $S$ , the relationship between  $L_i$  and  $K_{ij}$  can be written as

$$L_1 = \frac{1}{6S^2}(K_{33} - K_{11} + 3K_{22}), \quad (4)$$

$$L_2 = \frac{K_{11} - K_{22}}{S^2}, \quad (5)$$

$$L_{24} = \frac{K_{24}}{S^2}, \quad (6)$$

$$L_5 = 2L_1. \quad (7)$$

In Eqs. (4)–(7),  $S$  is the uniaxial scalar parameter expressing the magnitude of fluctuations about the director. It can be either positive or negative. The ensemble of molecules represented by  $Q$  tends to align along the director field when  $S$  is positive and tends to lie in the plane orthogonal to the director field when  $S$  is negative.

### B. Geometry system

The geometric model we use is a long cylindrical geometry of radius  $R$ , as shown in Fig. 1. The liquid crystal molecules are distributed in the cylinder, and the surface has degenerated planar boundary conditions. The standard cylindrical coordinate system  $(\rho, \varphi, z)$  is established, and the corresponding local frame  $\vec{e}_\rho, \vec{e}_\varphi, \vec{e}_z$  is also introduced. Here  $\vec{e}_z$  is along the symmetry axis,  $\vec{e}_\rho$  is the radial unit vector emanating from the symmetry axis, and  $\vec{e}_\varphi = \vec{e}_z \times \vec{e}_\rho$ .

The anchoring condition of the surface prevents the director from having an  $\vec{e}_\rho$  component, so  $\alpha(\rho = R) = \pm\pi/2$ .

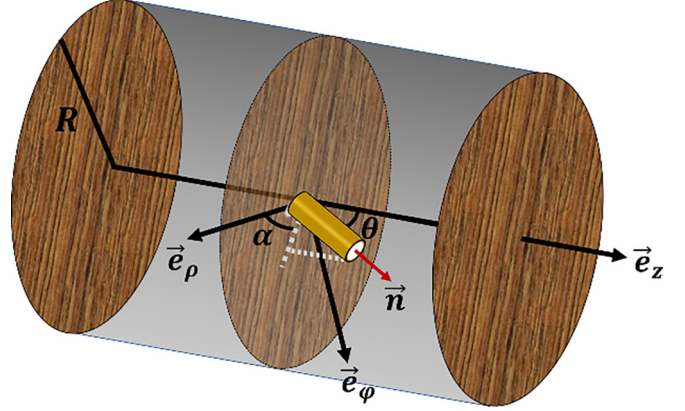


FIG. 1. Schematic diagram of the cylindrical geometry. Cylindrical coordinate system  $(\rho, \varphi, z)$  is to describe the configuration.  $\vec{n}$  is the director field,  $\theta$  is the angle between  $\vec{n}$  and the  $z$  axis, and  $\alpha$  is the angle between the  $\rho$ – $\varphi$  projection of  $\vec{n}$  and the  $\rho$  axis.  $R$  is the radius of the system.

Along the radial direction ( $\rho$  axis), we define a counterclockwise rotation of  $\vec{n}$  as right-handed, with  $\theta$  taking a positive value, while a clockwise rotation of  $\vec{n}$  as left-handed, with  $\theta$  taking a negative value, as shown in Fig. 2.

In addition, owing to the symmetry of a cylindrical system along the  $z$  axis, it is sufficient for us to illustrate the system changes by calculating one of the cross sections ( $\rho$ – $z$  plane). Thus, we could transfer the three-dimensional problem into a two-dimensional problem and improve the efficient of the numerical process.

### C. Scaling and dimensionless evolution equations

We introduced the following dimensionless quantities [26,37]:  $\tilde{f} \equiv f/[\frac{B^4}{(4C)^3}]$ ,  $\tilde{Q} \equiv Q/[\frac{B}{4C}]$ ,  $\kappa = \sqrt{\frac{q_0^4 CL_1}{B^2}}$ ,  $\tilde{\rho} \equiv 2q_0\rho$ ,  $\tilde{z} \equiv 2q_0z$ . Equations (1) and (2) can be reduced to

$$\tilde{f}_{\text{bulk}} = \frac{1}{12}\tilde{A}\text{tr}\tilde{Q}^2 - \frac{1}{3}\text{tr}\tilde{Q}^3 + \frac{1}{16}(\text{tr}\tilde{Q}^2)^2, \quad (8)$$

$$\tilde{f}_{\text{elastic}} = 2\kappa^2\{|\tilde{\nabla}\tilde{Q}|^2 + \tilde{L}_2|\tilde{\nabla} \cdot \tilde{Q}|^2 + \tilde{L}_{24}\tilde{\nabla} \cdot [(\tilde{\nabla}\tilde{Q})\tilde{Q} - \tilde{Q}\tilde{\nabla} \cdot \tilde{Q}] + \tilde{L}_5\tilde{Q} \cdot (\tilde{\nabla} \times \tilde{Q})\}. \quad (9)$$

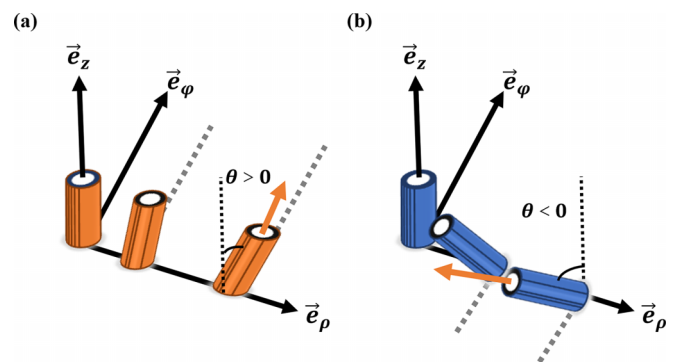


FIG. 2. (a) Right-handed twist structure; (b) left-handed twist structure.

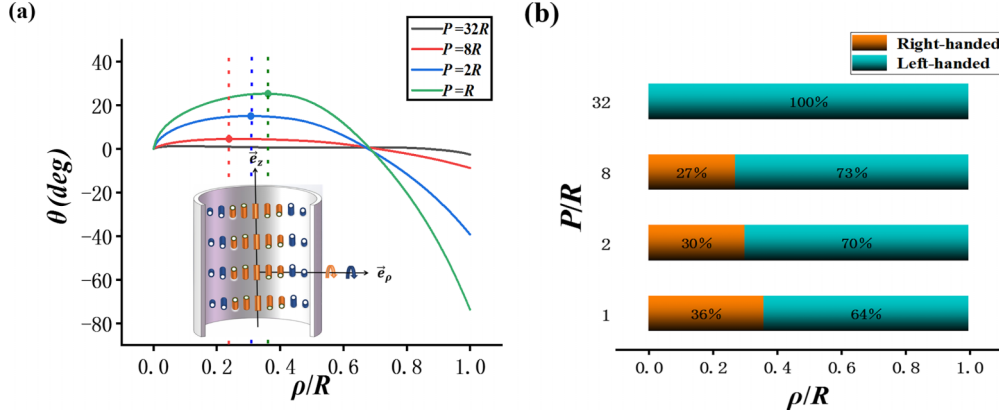


FIG. 3. (a) Twist structure induced by helical twisting power in a cylindrical cavity with  $K_{24} = 0$ . The inset shows the fine structure, where orange columns represent right-handed structure, and blue columns represent left-handed structure. (b) Regional distribution of two chiral structures with different values of  $P$ :  $P/R = 32, 8, 2, 1$ .

Equations (5)–(7) can be reduced to

$$\tilde{L}_2 = L_2/L_1 = \frac{6\left(\frac{K_{11}}{K_{33}} - \frac{K_{22}}{K_{33}}\right)}{3\frac{K_{22}}{K_{33}} + 1 - \frac{K_{11}}{K_{33}}}, \quad (10)$$

$$\tilde{L}_{24} = L_{24}/L_1 = \frac{6\frac{K_{24}}{K_{33}}}{3\frac{K_{22}}{K_{33}} + 1 - \frac{K_{11}}{K_{33}}}, \quad (11)$$

$$\tilde{L}_5 = L_5/L_1 = 2. \quad (12)$$

According to [38], the rescaled evolution equation for  $\tilde{Q}$  in the bulk can be obtained as follows:

$$\frac{\partial \tilde{Q}_{ij}}{\partial t} = \tilde{\Gamma} \left( -\frac{\delta \tilde{f}}{\delta \tilde{Q}} \right), \quad (13)$$

in which  $\tilde{\Gamma} = \Gamma \times \left(\frac{B^2}{4C}\right)$ ,  $\Gamma = 6D^*/[1-3\text{tr}(Q^2)]^2$ , and  $D^*$  is the rotational diffusion for the nematic.

The rescaled surface evolution equation based on  $\frac{\partial Q_s}{\partial t} = -\Gamma_s \left[ \frac{\partial f_s}{\partial Q_{ij}} + \frac{\partial f}{\partial (Q_{ij,k})} \tilde{v}_k \right]$  in the condition of  $f_s = 0$ , and  $\tilde{v}_k = \tilde{e}_\rho(\rho=R)$  on the surface, can be written as

$$\frac{\partial \tilde{Q}_s}{\partial t} = -\frac{1}{2q_0} \tilde{\Gamma}_s \left[ \frac{\partial \tilde{f}}{\partial (\tilde{Q}_{ij,\tilde{\rho}})} \right], \quad (14)$$

in Eq. (14),  $\tilde{\Gamma}_s = \Gamma_s \times \left(\frac{B^2}{4C}\right)$ . The rotational symmetry conditions at the cylindrical axis ( $\rho = 0$ ) give  $\tilde{Q}_{\rho\varphi} \equiv \tilde{Q}_{\rho z} \equiv \tilde{Q}_{\varphi z} \equiv 0$ ,  $\tilde{Q}_{\rho\rho,\rho} \equiv \tilde{Q}_{\varphi\varphi,\rho} \equiv \tilde{Q}_{zz,\rho} \equiv 0$ ,  $\tilde{Q}_{\rho\rho} \equiv \tilde{Q}_{\varphi\varphi} \equiv -\frac{1}{2}\tilde{Q}_{zz} \equiv 0$ .

### III. RESULTS

According to parameters given in [26,27],  $a = 0.195 \times 10^6 \text{ J/m}^3$ ,  $B = 7.155 \times 10^6 \text{ J/m}^3$ ,  $C = 8.82 \times 10^6 \text{ J/m}^3$ ,  $L_1 = 10.125 \times 10^{-12} \text{ J/m}$  are obtained. In our simulations, the scaled temperature is set to be  $\tilde{A} = 2/3$ . The rotational diffusion  $D^*$  is set to be  $0.35 \text{ m}^2/\text{N s}$ . For simplicity, the elastic constants  $K_{11} = K_{33} = K$ ,  $K_{22}/K = 0.1$  are chosen in our simulation, thus we can easily get  $\tilde{L}_2 = 18$  and the values of  $\tilde{L}_{24}$  for different values of  $K_{24}/K$  according to Eqs. (10) and (11). In this work, we focus on the chiral inversion induced by helical twisting power, combined with the effect of curved surface. As we know [12], the helical twisting power is inversely related to the pitch  $P$  for a given concentration of

liquid crystal material. Thus,  $P$  is used to characterize the helical twisting power in the following. The applied helical twisting power is left-handed in the following.

#### A. Chiral inversion in a cylindrical cavity with $K_{24} = 0$

When helical twisting power is applied to a cylindrical cavity with  $K_{24} = 0$ , it is surprising that two chiral twist structures appear simultaneously. Fig. 3(a) shows the fine structure after application of  $P$ . It can be seen that under the action of left-handed helical twisting power, a left-handed twist structure appears on the outer side, and a right-handed twist structure appears near the center of the cylinder. This behavior results from the curvature effect. On the outer side, geometric curvature is relatively small, and the chirality is more liable to the intrinsic helical. If the left-handed twist continues towards the central region with larger curvature, there would be a large bend cost due to the projection of the director on to the  $\rho$ - $\varphi$  plane, thus the left-handed twist is reduced and a right-handed twist structure appears as one approaches the center of the cylinder. In fact, the chiral inversion makes the small degree of  $\theta$  at small  $\rho$ , which can avoid the expensive bend energy with larger curvature. Figure 3(a) also gives that the angle of the revised right-handed twist structure increases with helical twisting force. In addition, the increase of helical twisting force is accompanied by the expansion of right-handed structure. Figure 3(b) shows the specific data.

#### B. Chiral inversion in a cylindrical cavity with $K_{24} \neq 0$

In Sec. III A, the curvature effect caused the chiral inversion structure in the action of helical twisting power. It is well known that nematics with  $K_{24} > 2K_{22}$  exhibit spontaneous distortion of two chiralities with equal probability [29,39–41]. Next, we explore the chiral inversion by the mutual competition between  $K_{24}$  and helical twisting power, using two spontaneous chiral twists induced by  $K_{24}$  as the ground state. The radius  $R$  of the cylindrical cavity and the anchoring conditions are consistent with above. The applied helical twisting power is left-handed and  $K_{24}/K = 0.4$ .

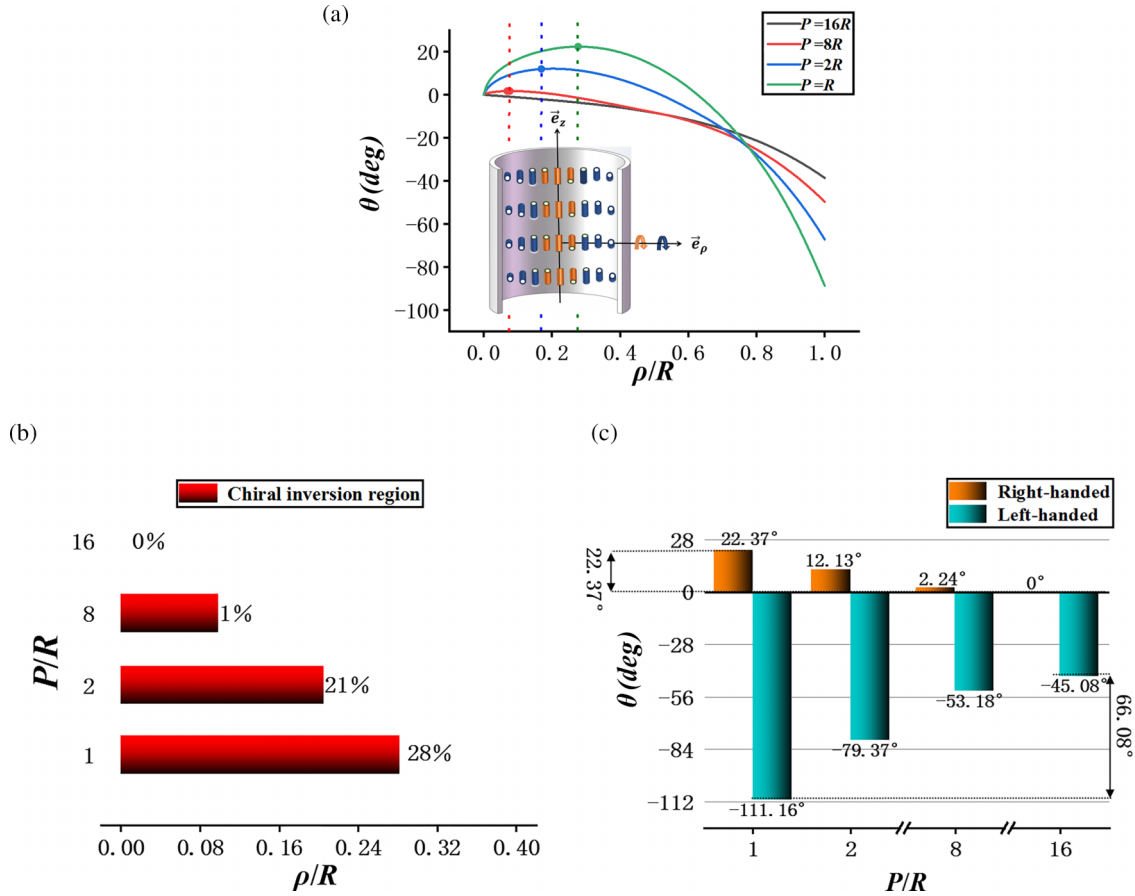


FIG. 4. (a) The twist structure in a cylindrical cavity with  $K_{24}/K = 0.4$  in the condition that the chirality of the spontaneous twist is the same as that of the applied helical twist power. The inset shows the fine structure of chiral reversal, where the orange columns represent the chiral inversion region. (b) Chiral inversion regions for different values of  $P$ :  $P/R = 16, 8, 2, 1$ . (c) Change of degree for two chiral structures with  $P/R = 16, 8, 2, 1$ .

### 1. Spontaneous twist is left-handed

In this section, the spontaneous chirality is consistent with the helical twisting power. For larger  $P$ , the effect of helical twisting power is small, thus the chirality structure is consistent with the spontaneous distortion without chiral reversal. As  $P$  decreases, chiral inversion occurs at a critical value corresponding to  $P = 16R$ . Figure 4(a) gives the profile of twist angle along  $\vec{e}_\rho$  for a chiral inversion structure, in which the inset shows the fine structure of chiral reversal. It is shown that chiral inversion occurs near the center.

Figure 4(b) demonstrates the regions of chiral inversion when  $P/R$  is 16, 8, 2, and 1, respectively. Apparently, the decrease of  $P$  causes the expansion of chiral inversion region from  $\rho = 0$  to  $\rho = 0.28R$ , and the adjustable range is 28%.

In addition, the twist degree is affected in the process of chiral inversion modulation, as shown in Fig. 4(c). The angle of the right-handed twist structure varies from  $0^\circ$  to  $22.37^\circ$ , with a regulation range of  $22.37^\circ$ ; while the angle of left-handed twist structure varies from  $-45.08^\circ$  to  $-111.16^\circ$ , with a range of  $66.08^\circ$ .

### 2. Spontaneous twist is right-handed

We further explored how the chiral reversal regulated by  $P$  in the condition that spontaneous chirality is right-handed,

opposite to the left-handed helical twisting power. Unlike the previous case, there is competition between  $K_{24}$  and helical twist power. At  $P = 3.53R$ , the effect of helical twist power exceeds  $K_{24}$  on the outer side, and there is a chiral inversion into the left-handed chiral structure near the lateral boundary, while the spontaneous right-handed distortion remains near the center [see Fig. 5(a)]. As  $P$  decreases, the dominate region of helical twist power increases, and the chiral inversion gradually extends from the boundary towards the central side. At  $P = 2.89R$ , the helical twist power is dominant in the whole system, and the system reach a maximum inversion region of  $0.8R$ , i.e., the adjustable range of chiral inversion is 80%, as shown in Figs. 5(a) and 5(b).

It should be pointed out that if  $P$  continues to decrease from  $2.89R$ , the net dominant effect of left-handed helical twist power will cause the expansion of right-handed structure and the area of left-handed twisted structure will decrease, which is consistent with Fig. 3(b); i.e., the area of chiral inversion will decrease. Thus the system has the largest chiral inversion region of  $0.8R$  at  $P = 2.89R$ .

The process of chiral inversion is accompanied by a change of twist degree. As shown in Fig. 5(c), with the decrease of  $P$ , the left-handed structure varies from  $0^\circ$  to  $71.04^\circ$ , with a modulation range of  $71.04^\circ$ ; and the right-handed structure varies from  $27.89^\circ$  to  $11.56^\circ$ , with a modulation range of  $16.33^\circ$ .

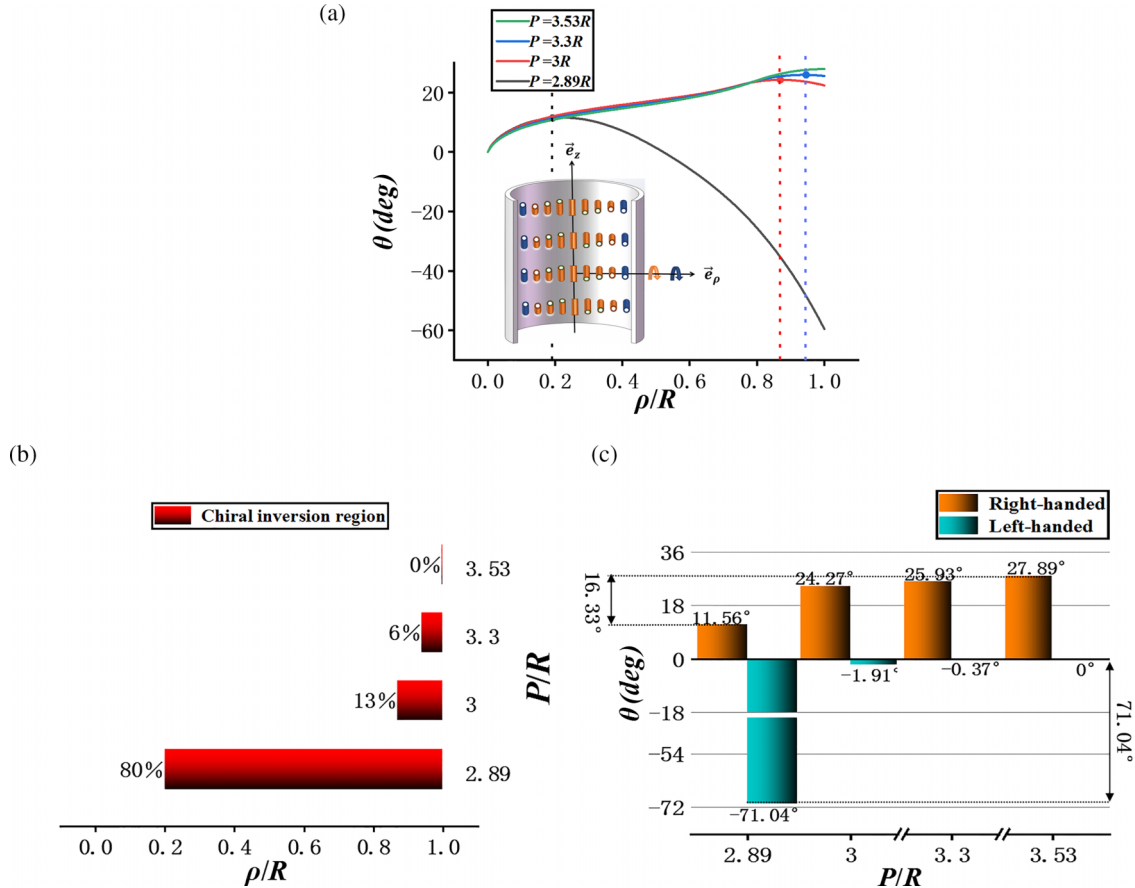


FIG. 5. (a) The twist structure in a cylindrical cavity with  $K_{24}/K = 0.4$  in the condition that the chirality of the spontaneous twist is opposite to that of the applied helical twist power. The inset shows the fine structure of chiral reversal, where the blue columns represent the chiral inversion region. (b) Chiral inversion regions for different values of  $P$ :  $P/R = 3.53, 3.3, 3, 2.89$ . (c) Change of degree for two chiral structures with  $P/R = 3.53, 3.3, 3, 2.89$ .

That is, the decrease of  $P$  enhances the left-handed twist structure, while it weakens the right-handed twist structure, which is reasonable. The variation of the distortion degree is not a continuous process, with an abrupt change at the point of maximum chiral inversion.

**C. Effect of  $K_{24}$  on the modulation of chiral inversion**

The results in Sec. III B indicate that the modulation of chiral inversion is more significant in the condition that the chirality of spontaneous twist is opposite to that of the applied helical twisting power. Thus, we focused on a cylindrical system with right-handed spontaneous twist and opposite left-handed helical twist power to investigate the effect of  $K_{24}$  on the chiral inversion.

Three values of  $K_{24}/K = 0.4, 0.6, \text{ and } 0.8$  are selected. Figure 6(a) shows chiral reversal regions with different  $K_{24}/K$ . It can be seen that the increase of  $K_{24}$  cause a reduction of the chiral reversal region, which is mainly related to the growing spontaneous twist structure by  $K_{24}$ . As we all know that a larger  $K_{24}$  is along with a greater spontaneous twist, so that the process of inducing a chiral reversal and the expansion of the reversal region requires a larger helical twisting power, i.e., a corresponding smaller  $P$ . According to the result in Sec. III A, the right-handed region expands and left-handed

region reduces as left-handed applied helical twist power  $P$  become smaller. Thus, larger  $K_{24}$  will induce a reduction of the reversal region.

In addition, the increase of  $K_{24}$  is accompanied by an increase of twist degree for both chiral structures, as shown in Fig. 6(b). For  $K_{24}/K = 0.8$ , the left and right chiral twisted structures vary between “ $0^\circ$  and  $107.03^\circ$ ” and “ $46.8^\circ$  and  $22.33^\circ$ ”, respectively, with the modulation range of  $107.03^\circ$  for left-handed structure and  $24.47^\circ$  for right-handed structure. The regulation ability of  $P$  to control the twist degree with  $K_{24}/K = 0.8$  is approximately 1.5 times that with  $K_{24}/K = 0.4$ . This is because a larger  $K_{24}$  needs a smaller  $P$  to induce chiral inversion, which directly results in a larger degree of twist structure.

**IV. CONCLUSION**

The chiral inversion phenomenon in cylindrical cavity with a degenerate planar anchoring is explored based on Landau–de Gennes theory. In the condition of ignoring  $K_{24}$ , an applied left-handed helical twisting power represented by  $P$  induces two chiral twist structures, with right-handedness near the center of the system and left-handedness on the outer. The region of right-handed structure expands with the increase of helical twisting force.

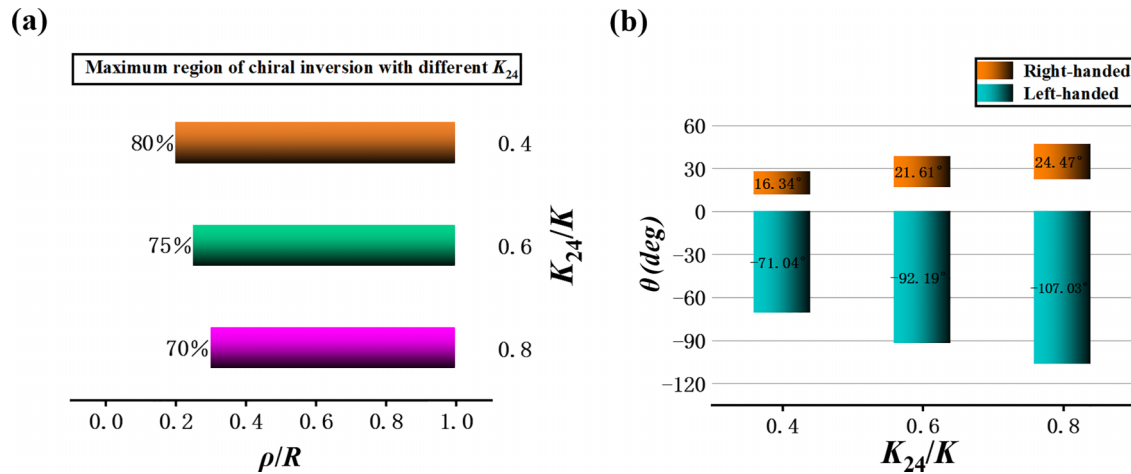


FIG. 6. The effect of  $K_{24}$  on chiral reversal, in the condition that the chirality of spontaneous right-handed twist is inverse with that of the left-handed helical twisting power,  $K_{24}/K = 0.4, 0.6, 0.8$ . (a) Chiral inversion regions when  $K_{24}$  takes different values. (b) The distortion degree for two twist structures when  $K_{24}$  takes different values.

The ability of  $P$  to modulate the chiral reversal on the basis of spontaneous twist is investigated with  $K_{24}/K = 0.4$  and applied left-handed helical twisting power. It is found that the spontaneous twist is more strongly modulated by  $P$  in cylindrical system with opposite spontaneous chirality to that of applied helical twisting power. Further, the values of  $K_{24}$  will affect the region of chiral separation, as well as the distortion degree for two twist structures.

The modulation of helical twisting power can be achieved by changing the optical environment experimentally [42,43], which means that CLC materials have the potential to be used in smart devices, for example, in light-controlled switches, due to the different response properties of different chiral twist structures to light, and that the movement of the chi-

ral inversion region can drive nanoparticle transport. Further research could be carried out on chiral inversions using curvature as a variable, in addition to extending the research model to more complex geometrical cylindrical shells, toroidal domains, and spheres, allowing for a variety of applications for CLCs.

#### ACKNOWLEDGMENTS

This work was supported by the National Natural Science Foundation of China Grant No. (11374087) and the National Science Foundation of Hebei Province of China Grant No. (F2020202015). All authors gave final approval for publication.

- [1] Y. Lu, Y. Yang, Y. Wang, L. Wang, J. Ma, L. Zhang, W. Sun, and Y. Liu, *Opt. Express* **26**, 3277 (2018).
- [2] Y. Han, K. Pacheco, C. W. Bastiaansen, D. J. Broer, and R. P. Sijbesma, *J. Am. Chem. Soc.* **132**, 2961 (2010).
- [3] M. A. White and M. LeBlanc, *J. Chem. Educ.* **76**, 1201 (1999).
- [4] Y. Jiang, R. Wilson, A. Hochbaum, and J. Carter, *Proc. SPIE* **4677**, 247 (2002).
- [5] E. N. Montbach, M. Lightfoot, and J. W. Doane, Inductive switching of cholesteric liquid crystal display device, U.S. Patent 9235096 (2016), <https://patents.google.com/patent/US9235096>.
- [6] C. Peng and O. D. Lavrentovich, *Soft Matter* **11**, 7257 (2015).
- [7] A. Darmon, O. Dauchot, T. Lopez-Leon, and M. Benzaquen, *Phys. Rev. E* **94**, 062701 (2016).
- [8] A. Darmon, M. Benzaquen, S. Čopar, O. Dauchot, and T. Lopez-Leon, *Soft Matter* **12**, 9280 (2016).
- [9] J. Ignés-Mullol, G. Poy, and P. Oswald, *Phys. Rev. Lett.* **117**, 057801 (2016).
- [10] T. Ogolla, S. B. Nashed, and P. J. Collings, *Liq. Cryst.* **44**, 1968 (2017).
- [11] L. Tran, M. O. Lavrentovich, G. Durey, A. Darmon, M. F. Haase, N. Li, D. Lee, K. J. Stebe, R. D. Kamien, and T. Lopez-Leon, *Phys. Rev. X* **7**, 041029 (2017).
- [12] T. Shirai, M. Shuai, K. Nakamura, A. Yamaguchi, Y. Naka, T. Sasaki, N. A. Clark, and K. V. Le, *Soft Matter* **14**, 1511 (2018).
- [13] T. Ogolla, R. S. Paley, and P. J. Collings, *Soft Matter* **15**, 109 (2018).
- [14] M. Mitov, *Adv. Mater.* **24**, 6260 (2012).
- [15] P.-G. De Gennes and J. Prost, *The Physics of Liquid Crystals* (Oxford University Press, Oxford, 1993).
- [16] P. M. Chaikin and T. C. Lubensky, *Principles of Condensed Matter Physics* (Cambridge University Press, Cambridge, UK, 1995).
- [17] Y. Yang, D. Zhou, X. Liu, Y. Liu, S. Liu, P. Miao, Y. Shi, and W. Sun, *Opt. Express* **28**, 31872 (2020).
- [18] A. Mujahid, H. Stathopoulos, P. A. Lieberzeit, and F. L. Dickert, *Sensors* **10**, 4887 (2010).
- [19] C.-K. Chang, C. W. Bastiaansen, D. J. Broer, and H.-L. Kuo, *Macromolecules* **45**, 4550 (2012).
- [20] J. Tang, J. Fang, Y. Liang, B. Zhang, Y. Luo, X. Liu, Z. Li, X. Cai, J. Xian, H. Lin *et al.*, *Sens. Actuators B* **273**, 1816 (2018).
- [21] L. Sutarlie, J. Y. Lim, and K.-L. Yang, *Anal. Chem.* **83**, 5253 (2011).
- [22] H. Coles and S. Morris, *Nat. Photonics* **4**, 676 (2010).

- [23] J. Beeckman, K. Neyts, and P. J. M. Vanbrabant, *Opt. Eng.* **50**, 081202 (2011).
- [24] J. Ortega, C. L. Folcia, and J. Etxebarria, *Materials* **11**, 5 (2017).
- [25] A. R. Fialho, N. R. Bernardino, N. M. Silvestre, and M. M. T. da Gama, *Phys. Rev. E* **95**, 012702 (2017).
- [26] L. Hou, S. Chen, X. Zhou, and Z. Zhang, *Liq. Cryst.* **47**, 950 (2020).
- [27] H. Zhao, Z. Zhang, J. Zhu, and X. Zhou, *Liq. Cryst.* **48**, 1120 (2021).
- [28] J. Eun, S.-J. Kim, and J. Jeong, *Phys. Rev. E* **100**, 012702 (2019).
- [29] K. Nayani, R. Chang, J. Fu, P. W. Ellis, A. Fernandez-Nieves, J. O. Park, and M. Srinivasarao, *Nat. Commun.* **6**, 8067 (2015).
- [30] J. Jeong, L. Kang, Z. S. Davidson, P. J. Collings, T. C. Lubensky, and A. Yodh, *Proc. Natl. Acad. Sci. USA* **112**, E1837 (2015).
- [31] K. Nayani, J. Fu, R. Chang, J. O. Park, and M. Srinivasarao, *Proc. Natl. Acad. Sci. USA* **114**, 3826 (2017).
- [32] J. Fu, K. Nayani, J. O. Park, and M. Srinivasarao, *NPG Asia Materials* **9**, e393 (2017).
- [33] A. Javadi, J. Eun, and J. Jeong, *Soft Matter* **14**, 9005 (2018).
- [34] P. G. de Gennes, J. Prost, and R. Pelcovits, *Phys. Today* **48**(5), 70 (1995).
- [35] P. Schiller, *Cryst. Res. Technol.* **31**, 616 (1996).
- [36] O. Guzman, N. L. Abbott, and J. J. de Pablo, *J. Chem. Phys.* **122**, 184711 (2005).
- [37] F. Fu and N. M. Abukhdeir, *Soft Matter* **13**, 4890 (2017).
- [38] A. N. Beris and B. J. Edwards, *Thermodynamics of Flowing Systems: With Internal Microstructure* (Oxford University Press, New York, 1994).
- [39] Z. S. Davidson, L. Kang, J. Jeong, T. Still, P. J. Collings, T. C. Lubensky, and A. Yodh, *Phys. Rev. E* **91**, 050501(R) (2015).
- [40] V. Koning, B. C. van Zuiden, R. D. Kamien, and V. Vitelli, *Soft Matter* **10**, 4192 (2014).
- [41] H. Mori, E. C. Gartland Jr., J. R. Kelly, and P. J. Bos, *Japan. J. Appl. Phys.* **38**, 135 (1999).
- [42] P. van de Witte, E. E. Neuteboom, M. Brehmer, and J. Lub, *J. Appl. Phys.* **85**, 7517 (1999).
- [43] M. T. Brannum, Functional performance of liquid crystalline elastomers, Ph.D. thesis, Case Western Reserve University, 2019.